Available online at www.sciencedirect.com

ScienceDirect

Solid Earth Sciences 5 (2020) 115−129

www.elsevier.com/locate/SESCI

Late Paleozoic to early Triassic granitoids from the Rudny Altai, Central Asian Orogenic Belt: Petrogenesis and implications for continental crustal evolution

Yunying Zhang [a,b,*], Pengfei Li [b], Min Sun [a], Chao Yuan [b]

[a] Department of Earth Sciences, The University of Hong Kong, Pokfulam Road, Hong Kong, China
[b] State Key Laboratory of Isotope Geochemistry, Guangzhou Institute of Geochemistry, Chinese Academy of Sciences, Guangzhou, 510640, China

Received 9 April 2020; revised 26 May 2020; accepted 27 May 2020
Available online 27 June 2020

Abstract

To better understand the continental crustal evolution in the Central Asian Orogenic Belt along the southwestern Siberian margin, a systematic study has been conducted on the late Paleozoic to early Triassic granitoids in the Rudny Altai. LA-ICP-MS zircon dating shows that granitoid magmatism in the study area can be divided into three episodes, i.e., middle to late Devonian, middle to late Carboniferous and early Triassic. Granitoids of the first two episodes have high SiO_2 (>70.0 wt.%), low MgO (<1.0 wt.%) and Ni (<3.1 ppm) contents, reflecting a crustal origin. Further, these samples exhibit variable Rb/Sr, CaO/Na_2O and Al_2O_3/TiO_2 ratios and variable $\varepsilon_{Nd}(t)$ (1.7−5.5) values, which, along with their metaluminous to weakly peraluminous compositions, imply a mixed crustal source involving clay-poor sediments and meta-basaltic components. In contrast, magmatism of the third episode possesses relatively low SiO_2 (63.2 wt.%) and high MgO (1.6 wt.%) but similar Ni (3.9 ppm) and $\varepsilon_{Nd}(t)$ (2.7). Its low Rb/Ba, Rb/Sr and Al_2O_3/TiO_2 ratios and metaluminous feature indicate a derivation from pre-existing basaltic crust. By integrating regional data, it is suggested that the Rudny Altai was generated by Devonian to late Carboniferous northeastward subduction of the Ob-Zaisan oceanic lithosphere. In detail, a retreating episode of subduction may occur in the Devonian, followed by a middle to late Carboniferous (330−318 Ma) normal subduction. In the late Carboniferous to early Permian (308−290 Ma), granitoids vanished in the Rudny Altai but widely intruded farther south into the Irtysh−Zaisan belt, probably in response to its collision with the Kazakhstan collage, pointing to that the Rudny Altai entered a syn-/post-collisional stage. Granitoids in the Permo-Triassic boundary (253−251 Ma) display features of intraplate granites, recording a period of intraplate epeirogeny.

Keywords: Granitoids; Petrogenesis; Continental crustal evolution; Rudny Altai; Central Asian orogenic belt

1. Introduction

The origin and secular evolution of the continental crust is a continuing matter of debate, although it is commonly accepted that most continental crust was produced in subduction zones (Chiaradia et al., 2014). As the main component of the continental crust, granitoids could provide crucial insights into the formation and evolution of the continental crust (Rapp and Watson, 1995; Barbarin, 1999; Annen et al., 2006), since specific source components and petrogenetic processes will produce distinctive types of granitoids. Generally speaking, partial melting of meta-sedimentary and meta-igneous rocks in the continental crust will create typical S-type and I-type granitoids, respectively (Chappell and White, 1992), while extreme fractionation of mantle magmas can generate A-type granitoids (Collins et al., 2020). Distinctive from S-, I- and A-type granitoids, another group of granitoids with high Ba

* Corresponding author. Department of Earth Sciences, The University of Hong Kong, Pokfulam Road, Hong Kong, China.
E-mail address: zyy518@hku.hk (Y. Zhang).
Peer review under responsibility of Guangzhou Institute of Geochemistry.

https://doi.org/10.1016/j.sesci.2020.05.001

(>500 ppm) and Sr (>300 ppm) contents was recognized by Tarney and Jones (1994) in the Scottish Caledonides. Granitoids of this type have been initially attributed to partial melting of subducted oceanic plateaus (Tarney and Jones, 1994) and subsequently attributed to partial melting of enriched lithospheric mantle (Eklund et al., 1998; Fowler et al., 2008) or mafic lower crust (Ye et al., 2008; Choi et al., 2009). In addition to the diversity of source materials, petrogenetic processes including magma segregation, transport and emplacement are also critical factors controlling the generation of granitoids in the continental crust (Petford et al., 2000; Brown, 2013). Accordingly, investigating the magma sources and magmatic processes of granitoids are pivotal to understanding the production and evolution of the continental crust.

The Central Asian Orogenic Belt (CAOB) is one of the largest accretionary orogenic belts on the Earth (Sengör et al., 1993; Windley et al., 2007; Xiao et al., 2015). Situated between the Siberian Craton to the north and the North China–Tarim cartons to the south, the CAOB was formed by long-lived amalgamation of juvenile terranes including island arc, accretionary wedge, ophiolite and oceanic plateau and a few continental fragments (Khain et al., 2003; Kröner et al., 2007; Wilhem et al., 2012). Granitoids with high positive whole-rock εNd(t) and zircon εHf(t) values are widespread in the CAOB, which represents an important site of crustal growth (Jahn et al., 2000; Xiao et al., 2008, 2015; Zhang et al., 2018). The Altai Mountain occupies the central-southern part of the CAOB, and extends ca. 2500 km from Russia, through Kazakhstan and NW China to S

W Mongolia (Windley et al., 2002; Safonova, 2014). This mountain belt is featured by abundant granitic intrusions (Yuan et al., 2007; Sun et al., 2008; Wang et al., 2009; Buslov et al., 2013; Tong et al., 2014; Cai et al., 2015), which allow us to characterize the evolution of regional continental crust. One of the least understood parts of the Altai Mountain is the Rudny Altai, where the magmatic sources, petrogenetic processes and geodynamic background of granitoids are poorly constrained, although some outstanding geochronological and geochemical studies have been conducted (Kuibida et al., 2013, 2020; Kuybida et al., 2015; Kruk et al., 2014). This study presents new geochronological, whole-rock geochemical and Sr–Nd isotopic results for the late Paleozoic to early Triassic granitoids from the Russian segment of the Rudny Altai, aiming to (1) investigate their origin and magmatic processes, and (2) constrain the associated geodynamic processes and evolutionary mechanisms of the regional continental crust.

2. Geological background and sample descriptions

2.1. Geological background

The NW–SE trending Rudny Altai extends from Russia to NE Kazakhstan. It is separated from the Neoproterozoic Gorny Altai island arc and the early Paleozoic Altai–Mongolian terrane to the northeast by the North–Eastern regional Fault and from the Irtysh–Zaisan Complex (also termed the Kalba–Narym terrane) to the southwest by the Irtysh Fault (Fig. 1a; Buslov et al., 2004; Safonova, 2014; Li et al., 2018). The Irtysh–Zaisan Complex is bounded with the Paleozoic Zharma–Saur and Chingis–Tarbagatai island arcs by the Char Shear Zone (Fig. 1a; Kruk et al., 2014; Kuibida et al., 2019). On a larger scale, the Char Shear Zone is merged into the Irtysh Fault in NW China, which bounds the Chinese Altai (part of the Altai–Mongolian terrane) with the Zharma–Saur arc in the West Junggar.

The Rudny Altai was developed along the southwestern margin of the Siberian accretionary system (i.e., the Gorny Altai island arc and Altai–Mongolian terrane) in response to late Paleozoic subduction of the Ob-Zaisan Ocean. The Rudny Altai has been considered as an arc-related extensional basin (i.e., back-arc basin) given the development of Devonian bimodal volcanics (Kuibida et al., 2020) and VMS-type Cu–Zn deposits (Buslov et al., 2004; Dyachkov et al., 2009; Lobanov et al., 2014; Safonova, 2014). Therefore, an "extensional accretionary orogen" comparable to that in the Lachlan Fold Belt in SE Australia has operated on the Rudny Altai (Collins, 2002). The Irtysh–Zaisan Complex, located farther south, is composed of ophiolitic fragments, volcanic rocks, clastic rocks and chert and has been thought to form in an accretionary wedge and to be overprinted by its collision with the Zharma–Saur island arc following the closure of the Ob-Zaisan Ocean (Sengör et al., 1993; Xiao et al., 2015; Li et al., 2017; Chen et al., 2019a,b). The oldest sedimentary strata in the Rudny Altai constitute the Silurian to early Devonian Korbalikha series, which consist mainly of interbedded sericite-chlorite schists, polymict metasandstones, phyllites and phyllitized shales (Kruk et al., 2014). The Korbalikha series are unconformably overlain by early to middle Devonian volcano-sedimentary sequences, which are further unconformably overlain by late Devonian shallow-marine clastic sediments and early Carboniferous carbonate-terrigenous strata. It is notable that the overlying section of the Carboniferous strata contain exclusively continental terrigenous sediments.

Granitoid rocks are widely emplaced in the Russian segment of the Rudny Altai (Fig. 1b), and can be roughly represented by eight independent igneous complexes based on geological observations and recent geochronological data: Aleisky (D_2), Pavlovsky (D_2), Zmeinogorsky (D_3), Ust'-Belovsky (D_3), Ust'yansky (D_3), Gilevsky (C_2), Volchikhinsky (C_2) and Sinyushensky (P_3–T_1) (Kruk et al., 2014). Lithologically, the granitoids of the Aleisky and Pavlovsky complexes are plagiogranite and biotite leucogranite, respectively, both of which belong to the granite–leucogranite association. The Zmeinogorsky complex, comprised of four phases (from early to late: (1) diorite, (2) amphibole-biotite plagiogranite, (3) biotite plagiogranite and (4) biotite plagioleucogranite), accounts for a major proportion of late Devonian intrusions in the Rudny Altai. The plagiogranites of this complex show low positive $\varepsilon_{Nd}(t)$ values (+1.1 to +1.8). The Ust'-Belovsky complex is made up of quartz diorite and granodiorite, while

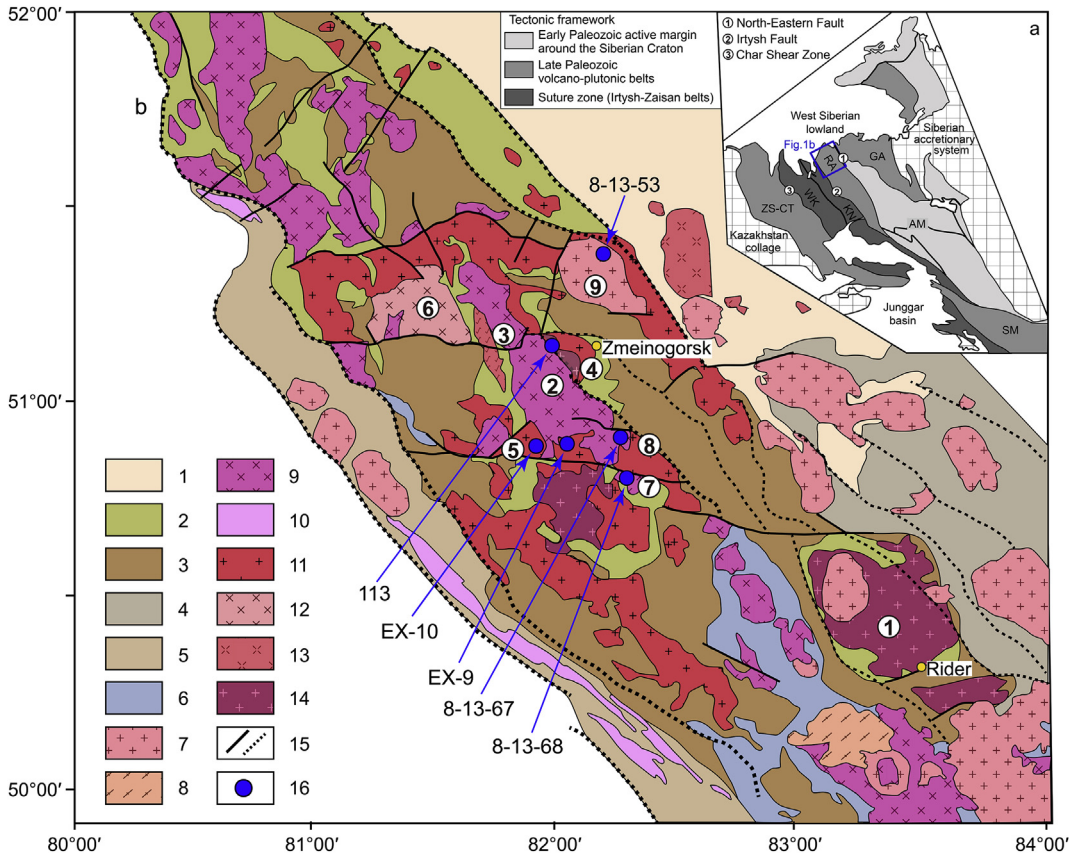

Fig. 1. (a) Simplified tectonic framework of the Altai accretionary-collision system (after Kuibida et al., 2020). Tectonic blocks: GA—Gorny Altai; RA—Rudny Altai; KN—Kalba Narym; WK—West Kalba; ZS-CT—Zharma Saur and Chingis Tarbagatai; AM—Altai Mongolian; SM—South Mongolian. (b) Sketch map of magmatic complexes in the Rudny Altai (modified after Kruk et al., 2014). 1: south-western margin of the Altai-Sayan folded area (Gorny Altai); 2: folded basement of the Rudny Altai; 3: subduction-related volcanic belt of the Rudny Altai; 4: Korgon-Holzun volcanic belt in the joint place of the Gorny and Rudny Altai; 5: deep-sea trench sediments; 6: continental deposits; 7: granitoids of the Leninogorsky, Sinyushensky and Kalbinsky complexes; 8: granitoids and volcanics of the Serzhikhinsky complex; 9: granitoids of the Gilevsky and Volchikhinsky complexes; 10: granitoids in the Irtysh shear zone; 11–14: granitoids of the Gorny and Rudny Altai (11 = Zmeinogorsky complex, 12 = Ust'yansky complex, 13 = Ust'-Belovsky complex; 14 = Aleisky complex); 15: faults; 16: samples. Numerals in circles mark massifs of ① = Leninogorsky, ② = Aleysky, ③ = Pavlovsky, ④ = Zmeinogorsky, ⑤ = Pervomaysky, ⑥ = Ust'yansky, ⑦ = Verkhneborovlyansky, ⑧ = Pervokamenksky and ⑨ = Sawushinsky.

the Ust'yansky complex is composed of granite. Granitoids of the Gilevsky complex were subjected to deformation and turned into mylonitic gneiss, which show relatively high $\varepsilon_{Nd}(t)$ value (+7.4; Kuibida et al., 2013). Rocks of the Volchikhinsky complex are mainly granodiorite and granite, which constitute a chain of linearly distributed bodies. The late Permian to early Triassic Sinyushensky complex includes three phases, namely from early to late the monzodiorite, the biotite granodiorite and the biotite granite.

2.2. Sample descriptions

Six granitic intrusions from the Russian segment of the Rudny Altai were sampled for petrological, geochronological and geochemical investigations in this study, and sample locations are shown on Fig. 1b. Samples EX-10 (Pervomaysky massif) and EX-9 (Ekaterinian massif) were collected from the Zmeinogorsky complex. The former is a coarse-grained monzogranite, which consists of anhedral quartz (~35 vol.%), subhedral to euhedral plagioclase (~30 vol.%), subhedral to anhedral orthoclase (~30 vol.%) and minor alkaline dark minerals (Fig. 2a), while the latter is a syenogranite, composed of anhedral quartz (~40 vol.%) and orthoclase (~35 vol.%), altered plagioclase (~25 vol.%) and minor aegirine (Fig. 2b).

Samples 8-13-68 (Verkhneborovlyansky massif) and 8-13-67 (Pervokamensky massif) were collected from the Volchikhinsky complex. The former is a medium-to coarse-grained biotite syenogranite, which contains anhedral quartz (~35 vol.%) and orthoclase (~45 vol.%) and subhedral plagioclase (~15 vol.%) with subordinate biotite (~5 vol.%) (Fig. 2c), while the latter is a coarse-grained monzogranite, made up of anhedral quartz (~25 vol.%), subhedral to euhedral plagioclase (~40 vol.%) and anhedral orthoclase (~35 vol.%) with minor biotite (Fig. 2d).

Sample 113 from the Aleisky complex is a coarse-grained syenogranite. It is composed of anhedral quartz (~40 vol.%), subhedral to euhedral plagioclase (~35 vol.%) and anhedral orthoclase (~20 vol.%) with minor biotite (Fig. 2e). Sample 8-13-53 from the Sawushinsky massif of the Sinyushensky

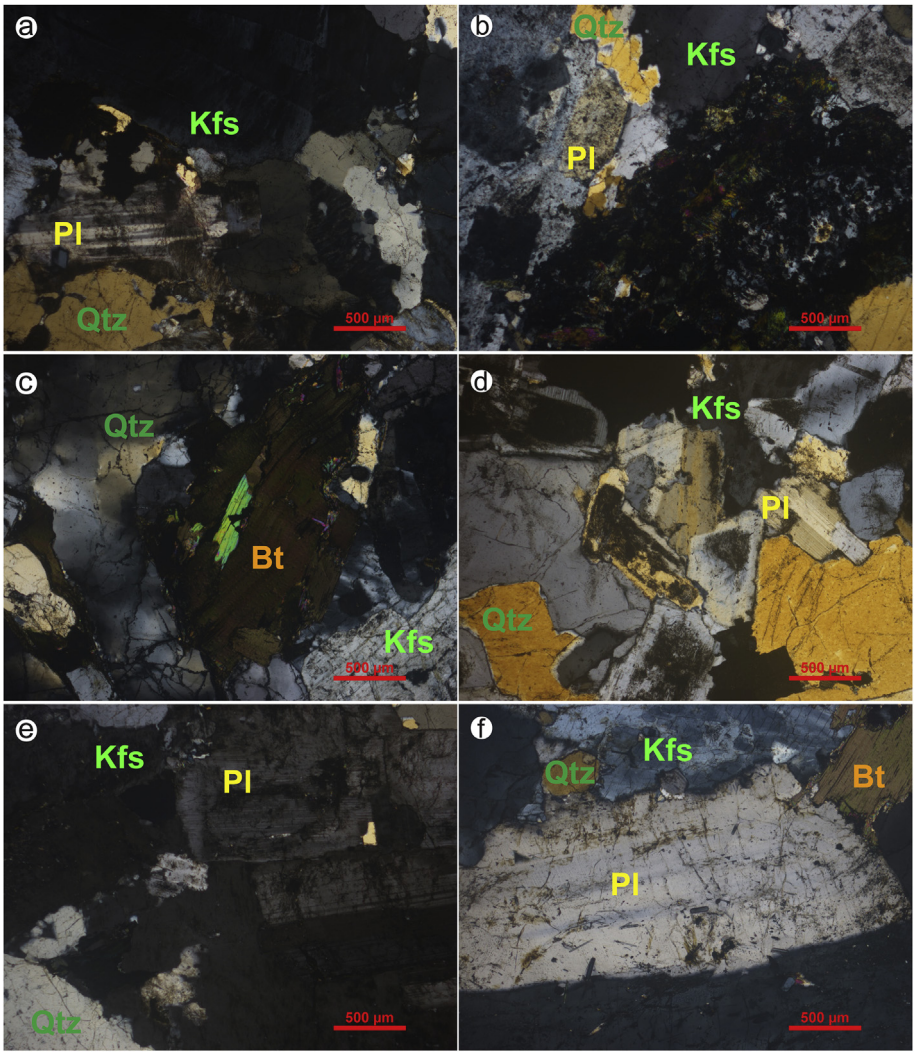

Fig. 2. Representative photomicrographs for the Devonian to Triassic granitoids from the Rudny Altai. (a) Sample EX-10 and (b) sample EX-9 from the Zmeinogorsky complex; (c) Sample 8-13-68 and (d) sample 8-13-67 from the Volchikhinsky complex; (e) Sample 113 from the Aleisky complex; (f) sample 8-13-53 from the Sinyushensky complex. Abbreviations: Pl, plagioclase; Kfs, K-feldspar; Qtz, quartz; Bt, biotite.

complex is a coarse-grained syenogranite, comprised of anhedral quartz (~20 vol.%), subhedral plagioclase (~35 vol.%) and anhedral orthoclase (~40 vol.%) with minor biotite (Fig. 2f).

3. Analytical methods

Zircon U–Pb dating and whole-rock Sr–Nd istotopic analyses were performed at the Wuhan Samplesolution Analytical Technology Co. Ltd. (Wuhan, China). The whole-rock major and trace element compositions were measured at the State Key Laboratory of Isotope Geochemistry, Guangzhou Institute of Geochemistry, Chinese Academy of Sciences (SKLIG GIG CAS).

3.1. Zircon U–Pb dating

Zircons were separated from the sampled granitoids using conventional heavy liquid and magnetic separation techniques and then were handpicked under a binocular microscope. Representative zircons were mounted in epoxy resin discs and polished to about half of their thickness. Zircon U–Pb dating was conducted by Laser Ablation Inductively Coupled Plasma Mass Spectrometry (LA-ICP-MS) using a GeolasPro laser ablation system coupled with a COMPexPro 102 ArF excimer laser (λ = 193 nm and maximum energy of 200 mJ). Helium was applied as a carrier gas, and argon was used as the make-up gas and mixed with the carrier gas via a T-connector before entering the ICP. Detailed operating conditions and analytical procedures are the same as described by Zong et al. (2017). Zircon 91500 and glass NIST610 were used as external calibration standards for zircon U–Pb isotopic and trace element analyses, respectively. Off-line selection and integration of back-ground and analysis signals, and time-drift correction and quantitative calibration for trace element analyses were calculated using the program ICPMSDataCal 7.2. Concordia diagrams and weighted mean calculations were made using the Isoplot 3.0 software (Ludwig, 2003).

3.2. Whole-rock geochemistry

Whole-rock major element oxides were determined using an X-ray fluorescence spectrometer (Rigaku 100e) on fused glass disks following the analytical procedures described by Li et al. (2006), and the analytical uncertainties were mostly between 1% and 5%. Trace elements, including rare earth elements (REE), high field strength elements (HFSE) and large ion lithophile elements (LILE), were measured by a Perkin-Elmer Sciex ELAN 6000 ICP–MS instrument, with analytical precision better than 5%. Rock powders (~40 mg) were digested in a mixture of HNO_3 and HF, within steel-bomb coated Teflon breakers for 48 h in order to achieve complete dissolution of refractory minerals. USGS rock standards (W-2a, BHVO-2 and AGV-1) and Chinese national rock standards (GSD-9, GSD-10, GSD-12, GSR-1, GSR-2 and SARM-4) were chosen for calibrating elemental contents of the analyzed samples.

3.3. Whole-rock Sr–Nd isotopes

Analyses of whole-rock Sr–Nd isotopes were performed on a Micromass Isoprobe multi-collecter mass spectrometer (MC-ICP-MS) following the procedures described by Gao et al. (2004). Sr and REEs were separated by ion-exchange columns packed with AG50W resins, and then Nd fractions were further separated with ion-exchange columns packed with LN resins. Measured $^{87}Sr/^{86}Sr$ and $^{143}Nd/^{144}Nd$ were normalized to $^{86}Sr/^{88}Sr = 0.1194$ and $^{146}Nd/^{144}Nd = 0.7219$, respectively. The $^{87}Sr/^{86}Sr$ ratio of the NBS987 standard and $^{143}Nd/^{144}Nd$ ratio of the Shin Etsu JNdi–1 standard measured during this study were 0.710235 ± 11 (2σ) and 0.512112 ± 9 (2σ), respectively. These values are identical to the reported results (0.710244 ± 14 (2σ) for NBS987 Sr standard and 0.512115 ± 7 (2σ) for JNdi-1 Nd standard) (Tanaka et al., 2000; Elburg et al., 2005).

4. Analytical results

4.1. Geochronology

LA-ICP-MS zircon U–Pb isotopic results for the studied granitoids are presented in Table S1. Zircons from sample 113 of the Aleisky complex are transparent and subhedral to euhedral with crystal lengths of 50–200 μm and aspect ratios of 1:1 to 1:3. The majority of these zircons are characterized by well-developed oscillatory zoning, which, together with their high Th/U ratios (0.29–0.82), suggests an igneous origin. The analyses of seventeen zircon grains from this sample give $^{206}Pb/^{238}U$ ages between 376 Ma and 394 Ma, yielding a weighted mean age of 385 ± 3 Ma (Fig. 3a), which is interpreted to record the crystallization age.

Samples EX-9 (Ekaterinian massif) and EX-10 (Pervomaysky massif) from the Zmeinogorsky complex were chosen for zircon U–Pb dating. Zircons from the former sample are subhedral to euhedral and transparent with sizes of 50–150 μm in length and length/width ratios of 1:1 to 3:1. Eighteen representative zircon grains with clear oscillatory zoning were analyzed and seventeen grains give concordant U–Pb ages with high Th/U ratios (0.26–0.48). Their $^{206}Pb/^{238}U$ ages range from 367 Ma to 382 Ma, which form a coherent cluster and yield a weighted mean age of 375 ± 2 Ma (Fig. 3b). Zircons from the latter sample are mostly stubby and have lengths of 50–100 μm with aspect ratios of 1:1 to 2:1. Eighteen ablation points from this sample yield Th/U ratios within 0.31–0.50 and concordant $^{206}Pb/^{238}U$ ages from 380 Ma to 387 Ma, which give a weighted mean age of 383 ± 2 Ma (Fig. 3c).

Samples 8-13-67 (Pervokamensky massif) and 8-13-68 (Verkhneborovlyansky massif) from the Volchikhinsky complex were processed for U–Pb isotopic analyses. Zircons from the former sample are transparent and mostly euhedral, and have lengths from 80 to 200 μm with aspect ratios of 1:1 to 5:1. All of the zircon grains exhibit clear oscillatory zoning, indicating a magmatic origin. Eighteen analyses yield high Th/U ratios between 0.33 and 0.67 and concordant $^{206}Pb/^{238}U$ ages between 313 Ma and 323 Ma, which form a population and give a weighted mean $^{206}Pb/^{238}U$ age of 320 ± 2 Ma (Fig. 3d). Zircons from the latter sample are prismatic and transparent with well-developed oscillatory zoning, suggesting a magmatic origin. The size of the zircons ranges from 50 to 150 μm in length, with aspect ratios of 1:1 to 3:1. The analyzed eighteen zircon grains give concordant U–Pb ages with high Th/U ratios (0.14–0.50). Among them, thirteen zircon points form a population with $^{206}Pb/^{238}U$ ages ranging from 325 Ma to 337 Ma, which yield a weighted mean age of 330 ± 3 Ma (Fig. 3e). The remaining five zircons give relatively old ages (348–371 Ma), which probably represent ages of inherited zircons.

Zircons from sample 8-13-53 (Sawushinsky massif of the Sinyushensky complex) are stubby to prismatic and transparent, and have lengths from 100 to 300 μm with length/width ratios of 1:1 to 3:1. These zircons exhibit clear oscillatory zoning, consistent with an igneous origin. Seventeen of eighteen analyzed zircons give concordant U–Pb ages with Th/U ratios within 0.47–0.63. Their $^{206}Pb/^{238}U$ ages range from 244 Ma to 255 Ma, yielding a weighted mean age of 251 ± 2 Ma (Fig. 3f). This age is slightly older than the Ar–Ar age (244 ± 1 Ma) obtained on biotite from the same pluton (Kruk et al., 2014 and references therein), suggesting that the zircon age of this study is the best estimation for emplacement age of the Sawushinsky massif.

Collectively, the studied granitic intrusions were emplaced within three stages, the first in the middle to late Devonian (385–375 Ma), the second in the Carboniferous (330–320 Ma) and the third in the early Triassic (ca. 251 Ma).

4.2. Major and trace elements

Bulk-rock major and trace element compositions of the analyzed granitoids are presented in Table S2, which overlap with previously reported data from the Rundy Altai (e.g., Kuibida et al., 2013, 2020; Kuybida et al., 2015; Kruk et al.,

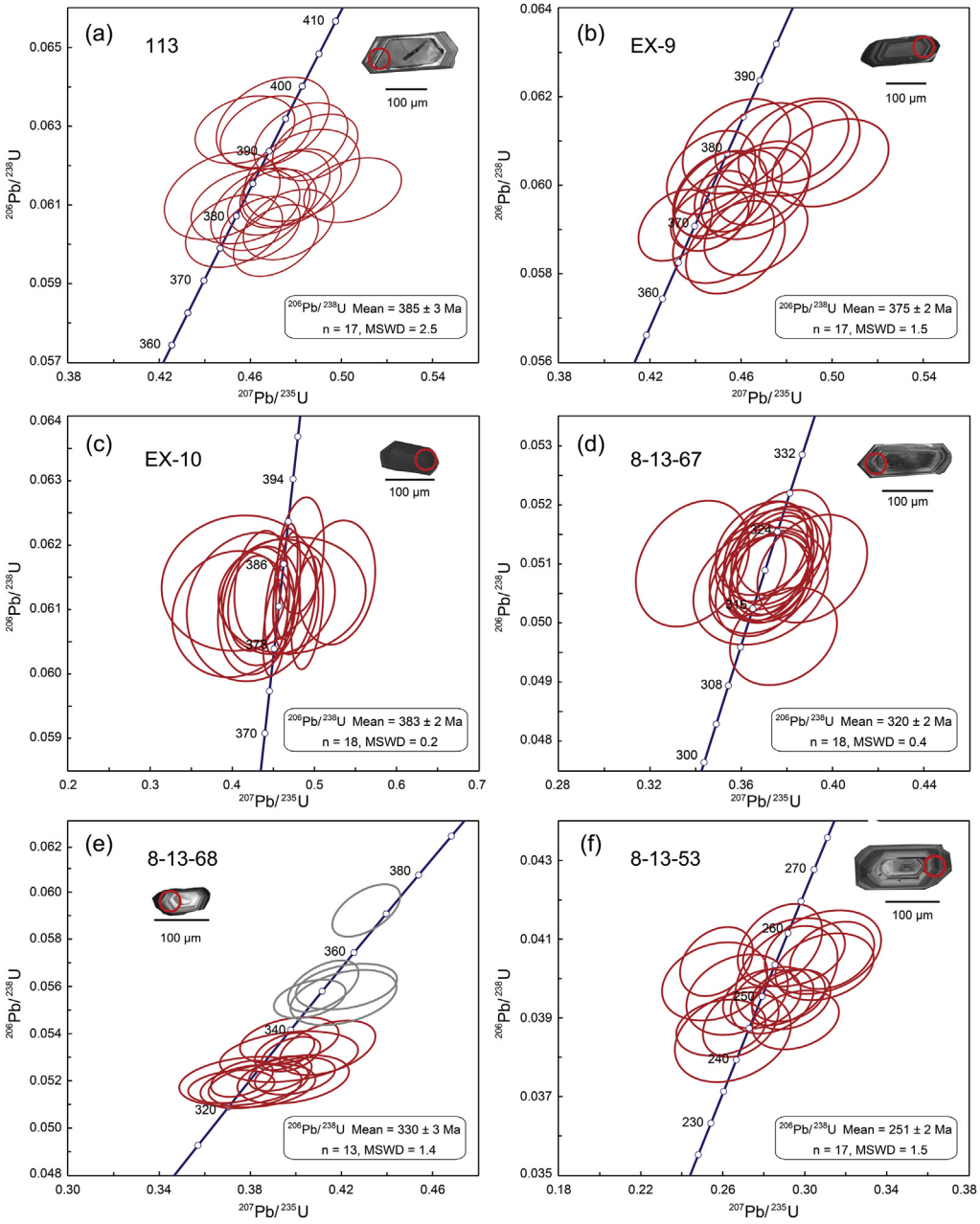

Fig. 3. LA-ICP-MS zircon U–Pb concordia diagrams for the studied granitoids: (a) sample 113 from the Aleisky complex; (b) sample EX-9 and (c) sample EX-10 from the Zmeinogorsky complex; (d) sample 8-13-67 and (e) sample 8-13-68 from the Volchikhinsky complex; (f) sample 8-13-53 from the Sinyushensky complex.

2014). The loss on ignition of all the studied granitoids is less than 0.70 wt.%, indicating that these samples are fresh.

4.2.1. Devonian granitoids

The Devonian granitoids have high SiO_2 (73.1–77.1 wt.%), low MgO (0.13–0.89 wt.%) and $Fe_2O_3^T$ (1.20–1.74 wt.%) contents (Fig. 4a), with Na_2O/K_2O ratios between 1.63 and 7.51. Their variable K_2O (0.51–2.94 wt.%) contents indicate a spread from low-K tholeiitic to medium-K calc-alkaline compositions (Fig. 4b). In addition, the studied Devonian granitoids show metaluminous characteristics with A/CNK (molar $Al_2O_3/[K_2O + Na_2O + CaO]$) values from 0.89 to 1.04 (Fig. 4c). Such A/CNK values are consistent with those of previously investigated Devonian granitoids (Kruk et al., 2014).

Samples of the Devonian granitoids have variable concentrations of Sr (55.5–360 ppm), Rb (5.01–77.2 ppm) and Ba (151–511 ppm), and possess low Rb/Ba (0.03–0.15) and variable Rb/Sr (0.01–1.39) ratios. These rocks are featured by light REE (LREE) enrichment ($[La/Sm]_N$ = 1.92–2.68; $[La/Yb]_N$ = 2.10–3.02) and negligible heavy REE (HREE) fractionation ($[Gd/Yb]_N$ = 0.82–1.07) with variable Eu anomalies (δEu = 0.34–1.03) (Fig. 5a). On the primitive mantle–normalized trace element diagrams, the Devonian

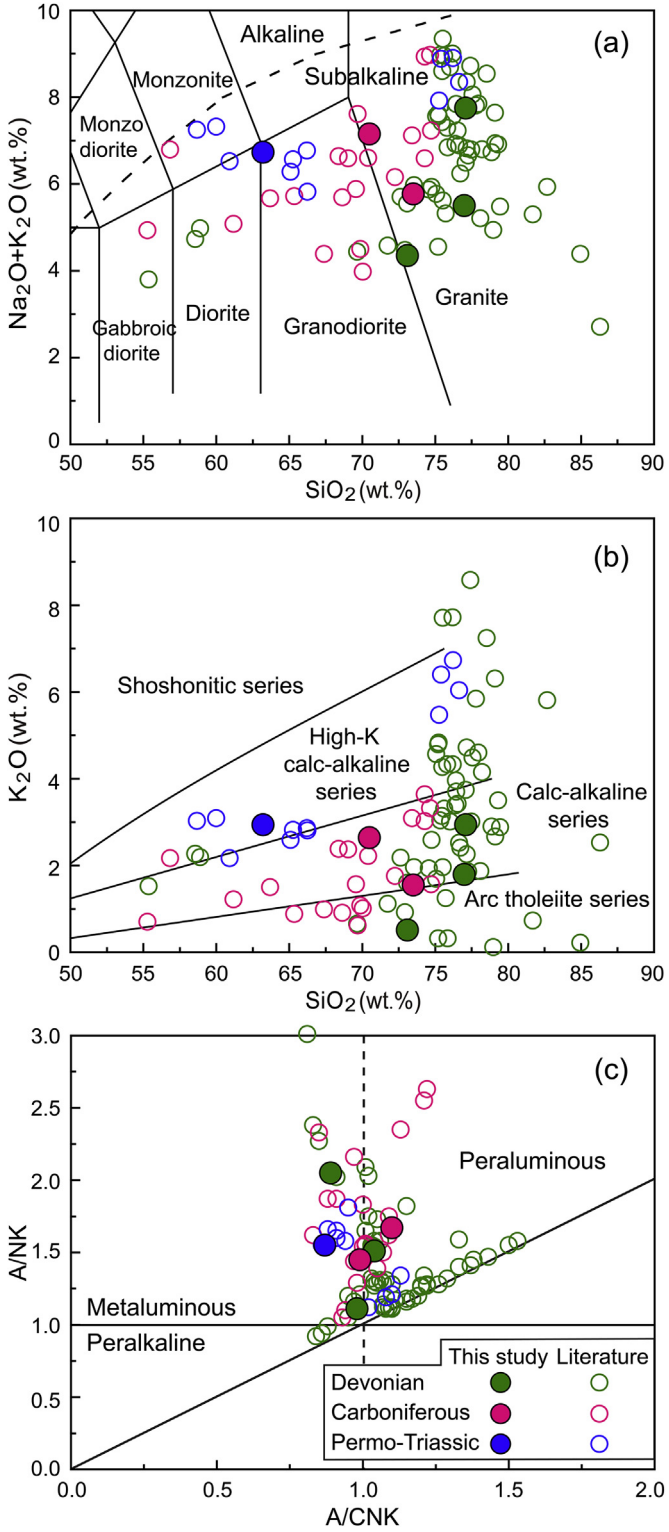

Fig. 4. Petrochemical diagrams of the Devonian to Triassic granitoids in the Rudny Altai. (a) Total alkali–silica (TAS) diagram (Le Bas et al., 1986); (b) K_2O–SiO_2 diagram (Peccerillo and Taylor, 1976); (c) A/NK–A/CNK diagram (Maniar and Piccoli, 1989). Previous data for the Devonian, Carboniferous and Permo-Triassic granitoids in the Rudny Altai are from Kruk et al. (2014), Kuibida et al. (2013, 2020) and Kuybida et al. (2015).

granitoids show relative enrichment in LILEs (e.g., Ba) and depletion in HFSEs (e.g., Nb and Ta) (Fig. 5b).

4.2.2. Carboniferous granitoids

The Carboniferous granitoids possess SiO_2 between 70.5 and 73.5 wt.% (Fig. 4a), with relatively high TiO_2 (0.23–0.41 wt.%) and Al_2O_3 (14.4–14.9 wt.%) contents. They are relatively Na-rich, as suggested by high Na_2O (4.22–4.51 wt.%) contents and high Na_2O/K_2O (1.71–2.71) ratios. Samples of the Carboniferous granitoids have K_2O contents of 1.55–2.64 wt.% and thus are classified as medium-K calc-alkaline series in the SiO_2–K_2O diagram (Fig. 4b), and exhibit metaluminous to weakly peraluminous characteristics ($0.99 < A/CNK < 1.10$) (Fig. 4c).

The Carboniferous granitoid samples are characterized by low Zr (59.2–66.2 ppm) and Nb (2.88–4.72 ppm) contents, low Nb/Ta (8.96–10.0), Rb/Ba (0.12–0.23) and Rb/Sr (0.18–0.27) ratios. Furthermore, they display moderate LREE enrichment ($[La/Sm]_N = 2.08–3.53$; $[La/Yb]_N = 2.60–8.97$), with slight HREE fractionation ($[Gd/Yb]_N = 0.99–1.57$) and weak Eu anomalies ($\delta Eu = 0.79–0.87$) (Fig. 5c). In the primitive mantle-normalized multi-element diagrams, the Carboniferous rocks show enrichment in LILEs (e.g., Rb and U) relative to HFSEs (e.g., Nb) (Fig. 5d).

4.2.3. Triassic granitoids

The Triassic granitoid sample is granodioritic in composition (Fig. 4a). Compared to the Devonian and Carboniferous granitoids, it has lower SiO_2 (63.2 wt.%), but higher TiO_2 (1.20 wt.%), $Fe_2O_3^T$ (7.03 wt.%) and CaO (4.05 wt.%) contents. The granodiorite sample is relatively Na-rich, as indicated by high Na_2O (3.80 wt.%) content and high Na_2O/K_2O (1.29) ratio, and plots into the field of high-K calc-alkaline series on the SiO_2–K_2O plot (Fig. 4b). Moreover, this sample exhibits metaluminous composition with A/CNK value of 0.87 (Fig. 4c).

The Triassic granodioritic sample has high Zr (261 ppm), Nb (36.4 ppm) Y (112 ppm), Ba (1149 ppm), Sr (390 ppm) and total REE (549 ppm) contents. In addition, this sample is characterized by relatively low Rb/Ba (0.06) and Rb/Sr (0.19) but high 10,000*Ga/Al (3.0) ratios. Similar to the Devonian and Carboniferous granitoids, this sample shows moderate LREE enrichment ($[La/Sm]_N = 2.28$; $[La/Yb]_N = 5.65$) and slight HREE fractionation ($[Gd/Yb]_N = 1.67$), with moderate Eu anomaly ($\delta Eu = 0.60$) (Fig. 5e). In primitive mantle normalized trace element spider-diagram, it displays depletion of HFSEs such as negative Nb and Ta anomalies, but enrichment of LILEs such as positive Ba and U anomalies (Fig. 5f).

4.3. Sr–Nd isotopic compositions

The Sr–Nd isotopic compositions of the studied Devonian to Triassic granitoids are presented in Table S3 and Fig. 6. The Devonian granitoids have relatively lower $\varepsilon_{Nd}(t)$ values (1.7–2.3) and older two-stage Nd model ages ($T_{DM2} = 0.95–1.0$ Ga) than those of the Carboniferous

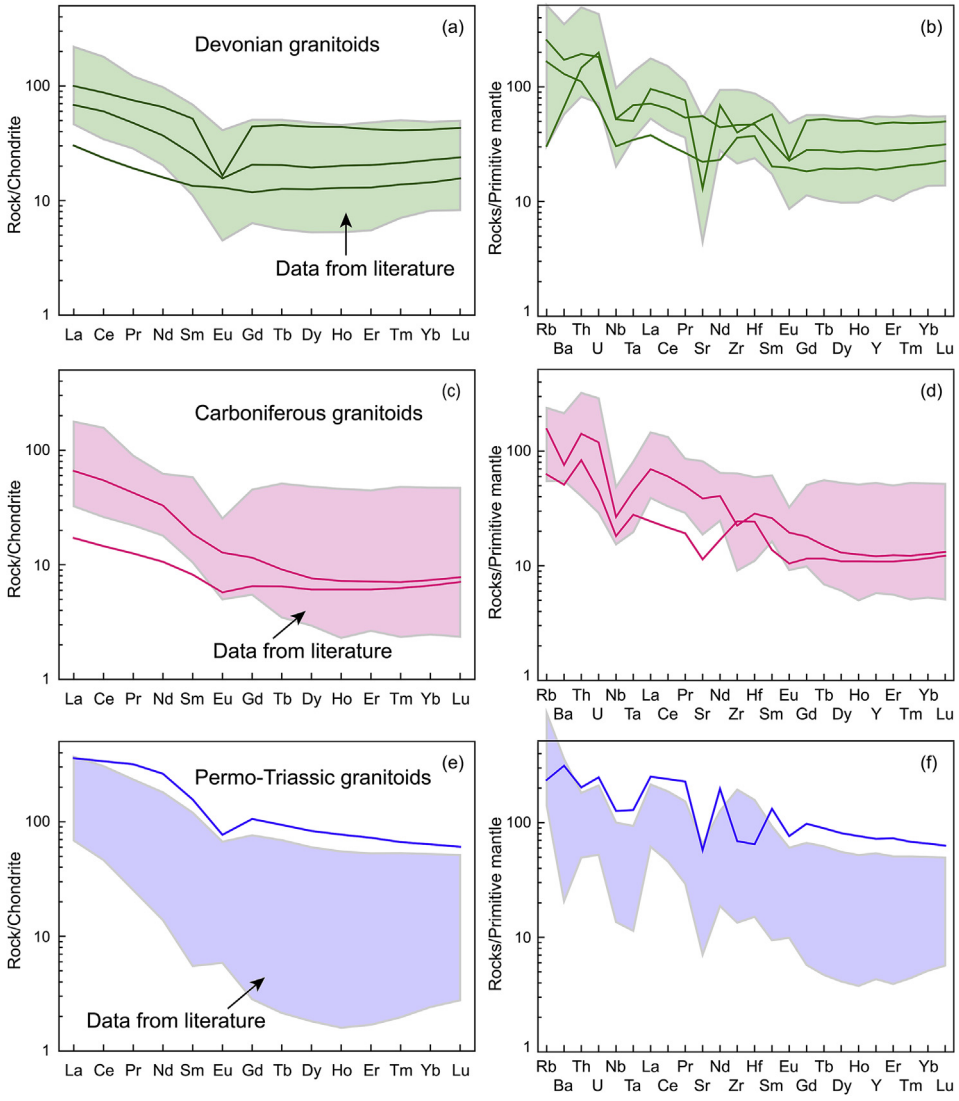

Fig. 5. Chondrite-normalized REE patterns (a–c) and primitive mantle-normalized multi-element patterns (d–f) for the Devonian to Triassic granitoids in the Rudny Altai. Normalizing values are from Sun and McDonough (1989). Fields for previous Devonian, Carboniferous and Permo-Triassic granitoids in the Rudny Altai are from Kruk et al. (2014), Kuibida et al. (2013, 2020) and Kuybida et al. (2015).

granitoids ($\varepsilon_{Nd}(t)$ = 4.5–5.5; T_{DM2} = 0.64–0.73 Ga) and Triassic granodiorite ($\varepsilon_{Nd}(t)$ = 2.7; T_{DM2} = 0.82 Ga). As shown in the Sr–Nd isotopic diagram (Fig. 6a), the initial $^{87}Sr/^{86}Sr$ ratios of the Carboniferous ($^{87}Sr/^{86}Sr_i$ = 0.7040–0.7044) and Triassic ($^{87}Sr/^{86}Sr_i$ = 0.7052) granitoids fall well within the range of Devonian samples ($^{87}Sr/^{86}Sr_i$ = 0.7030–0.7063). Moreover, their $\varepsilon_{Nd}(t)$ values are generally similar to those of previously published data for the granitoids in the Rudny Altai (Fig. 6b; Kuibida et al., 2013, 2020; Kruk et al., 2014).

5. Discussion

5.1. Geochronological and geochemical frameworks of the Rudny Altai granitoids

Our new isotopic dating results (n = 6), together with published zircon data of granitoids and their eruptive equivalents in the Rudny Altai (n = 20), are compiled in a histogram (Fig. 7). It shows a prolonged granitic magmatism in this region (395–251 Ma). Three magmatic episodes, encompassing the middle to late Devonian (395–371 Ma), the middle to late Carboniferous (330–318 Ma) and the late Permian to early Triassic (253–251 Ma), and two apparent gaps of 371–330 Ma and 318–253 Ma are recognized. Our zircon ages of this study correspond to the three episodes.

The striking features for granitoids of the Devonian episode are that most rocks have high silica contents (SiO_2 > 75 wt.%) (Fig. 4a) and show strongly peraluminous features (A/CNK > 1.1) (Fig. 4c). In contrast, most rocks of the Carboniferous and Permian to Triassic episodes have SiO_2 < 75 wt.% (Fig. 4a) and exhibit metaluminous to weakly peraluminous characteristics (Fig. 4c). As shown on the SiO_2–K_2O diagram (Fig. 4b), the Devonian rocks show a wide range from low-K tholeiitic to medium-K and high-K calc-

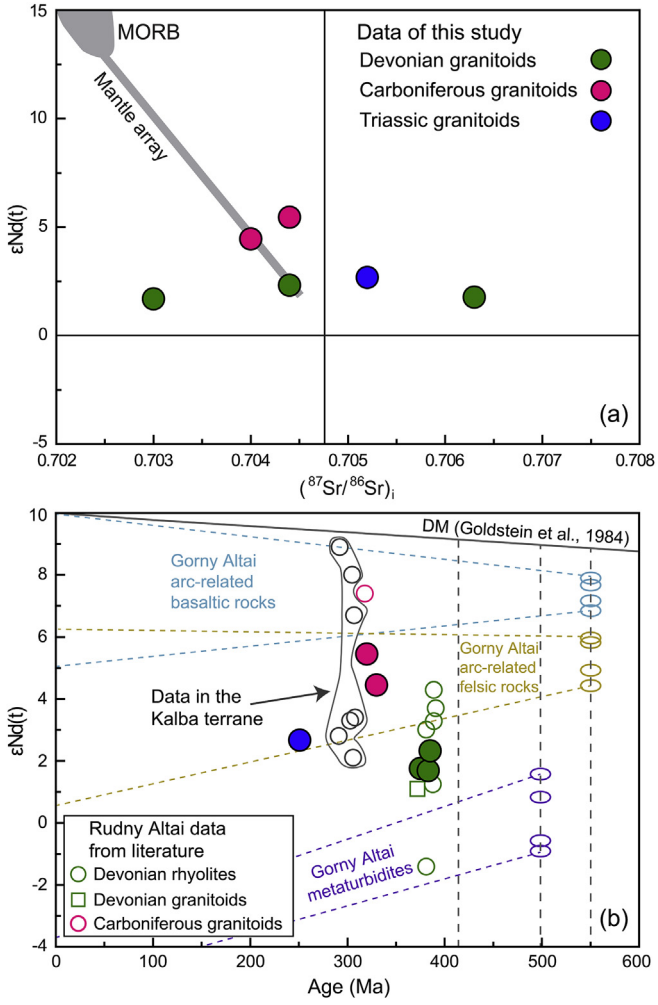

Fig. 6. (a) $\varepsilon_{Nd}(t)$ versus $(^{87}Sr/^{86}Sr)_i$ and (b) $\varepsilon_{Nd}(t)$–Age diagrams for the granitoids from the Rudny Altai. Rudny Altai data from literature in (b) are from Kruk et al. (2014) and Kuibida et al. (2013, 2020), data from the Kalba terrane in (b) are from Kuibida et al. (2019), and data from the Gorny Altai in (b) are from Kruk et al. (2010) and Kruk (2015). The DM line is taken from Goldstein et al. (1984).

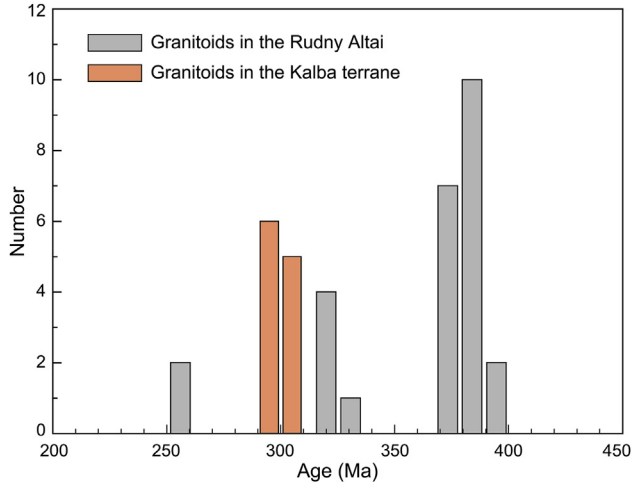

Fig. 7. Histogram of zircon U–Pb ages for granitoids in the Rudny Altai and Kalba terrane. The Rudny Altai data from literature are from Kruk et al. (2014), Kuibida et al. (2013, 2020) and Kuybida et al. (2015). The age data in the Kalba terrane are from Kuibida et al. (2009, 2019) and Khromykh et al. (2018).

alkaline series, whereas the Carboniferous and Permian to Triassic rocks mainly belong to medium-K and high-K calc-alkaline series, respectively. The above compositional differences may suggest that they were originated from different sources and formed in different tectonic settings.

5.2. Petrogenesis of the Devonian to Triassic granitoids

Granitoids are generally classified as I-, S- and A-type granites with distinctive mineral assemblage, geochemical composition and petrological process (Whalen et al., 1987; Chappell and White, 1992). I-type granites often contain typical minerals such as amphibole and show metaluminous to weakly peraluminous compostions with relatively low ASI values; whereas S-type granites usually contain typical aluminous minerals such as garnet, cordierite and muscovite and exhibit strongly peraluminous compostions with high ASI values. As for A-type granites, they commonly involve Fe-rich mafic silicates and are characterized by alkaline and peralkaline compositions with high Zr, Nb, Ce and Y and low Sr and Ba contents and high Ga/Al and Fe/Mg ratios (Bonin, 2007). Both the Devonian and Carboniferous rocks of this study are featured by low ratios of Ga/Al and FeO^T/MgO and low contents of Zr + Nb + Ce + Y (Fig. 8a and b), clearly precluding affinities to A-type granites. Instead, the Devonian (A/CNK = 0.89 to 1.04) and Carboniferous (A/CNK = 0.99 to 1.10) granitoids of this study display metaluminous to weakly peraluminous features, reflecting geochemical affinities to I- and S-type granites and indictaing that both meta-igneous and meta-sedimentary materials were involved in their sources. In contrast, the Triassic sample has relatively high Ga/Al and FeO^T/MgO ratios and high concentrations of Zr + Nb + Ce + Y (Fig. 8a and b), resembling those of A-type granitic rocks. However, distinctively different from typical A-type granites, the Triassic sample has low SiO_2 (63.2 wt.%) and high Ba (1149 ppm) and Sr (390 ppm) contents, which make them akin to high Ba–Sr granitoids (Tarney and Jones, 1994; Fowler et al., 2001). For this reason, we tentatively consider that the Triassic granodiorite shares a common petrological process with high Ba–Sr granitoids.

The Devonian (SiO_2 = 73.1–77.1 wt.%, MgO = 0.13–0.89 wt.%, Cr < 5.0 ppm and Ni < 3.0 ppm) and Carboniferous (SiO_2 = 70.5–73.5 wt.%, MgO = 0.54–0.92 wt.%, Cr < 15.6 ppm and Ni < 3.1 ppm) granitoids of this study possess high Si and low Mg, Cr and Ni contents (Table S2), suggesting a crustal rather than mantle source. Melts of meta-igneous rocks are featured by high CaO but low Al_2O_3 and Rb contents as well as high CaO/Na_2O but low Al_2O_3/TiO_2, Rb/Ba and Rb/Sr ratios, while melts of meta-sedimentary suites have the opposite compositions (Sylvester, 1998; Jung and Pfänder, 2007). For the Devonian and Carboniferous granitoids, they exhibit variable Rb/Sr, CaO/Na_2O and Al_2O_3/TiO_2 ratios (Fig. 8c and 8d), thus

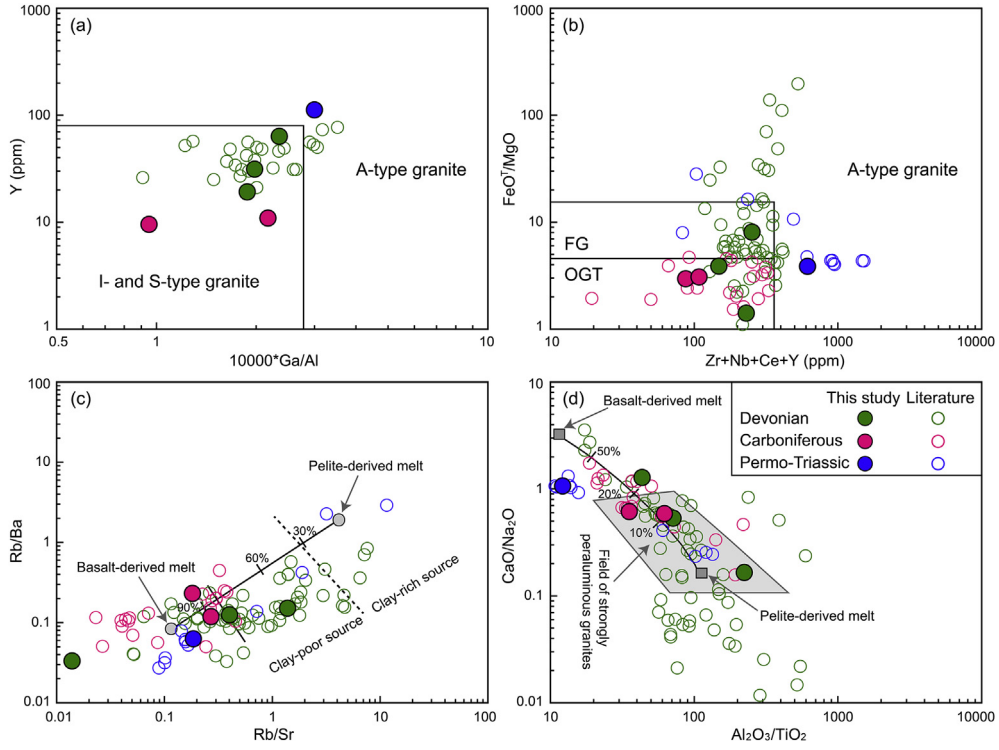

Fig. 8. (a) Y–Ga/Al*10,000 and (b) FeO^T/MgO–(Zr + Nb + Ce + Y) diagrams (after Whalen et al., 1987) for the granitoids in the Rudny Altai; FG represents fractionated granite and OGT represents unfractionated M–, I- and S-type granite. (c) Rb/Ba–Rb/Sr and (d) CaO/Na_2O–Al_2O_3/TiO_2 plots (after Sylvester, 1998) for the granitoids in the Rudny Altai; Both the mixing curves between basalt- and pelite-derived melts and field of strongly peraluminous granites are from Sylvester (1998). Rudny Altai data from literature are from Kruk et al. (2014), Kuibida et al. (2013, 2020) and Kuybida et al. (2015).

demonstrating a mixed source involving clay-poor sediments and meta-basaltic components, consistent with their metaluminous to weakly peraluminous characteristics. To identify their possible sources, it is necessary to compare the isotopic compositions of the studied granitoids with those of crustal rocks in the surrounding regions. As shown on the εNd(t)–Age diagram (Fig. 6b), both the Devonian and Carboniferous granitoids fall between the metaturbidites and arc-related basalts from the Gorny Altai (Kruk et al., 2010; Kruk, 2015), suggesting that these two components are potential candidates for their sources. Both two components could be transported in the Altai Mountain and deposited prior to Devonian and Carboniferous granitic magmatism. Moreover, the Devonian granites have relatively lower $\varepsilon_{Nd}(t)$ values (1.7–2.3) and older two-stage Nd model ages (0.95–1.0 Ga) than those of Carboniferous granites ($\varepsilon_{Nd}(t)$ = 4.5–5.5 and T_{DM2} = 0.64–0.73 Ga), which indicate that the magma sources of the Devonian granites involved more recycled sediments. This inference agrees with the fact that some samples from the Devonian granites have the highest Al_2O_3/TiO_2 and Rb/Sr ratios among the Devonian and Carboniferous granites (Fig. 8c and 8d).

As mentioned above, the Triassic granodiorite resembles high Ba–Sr granitoids (Fig. 9a), which is further confirmed by its high K/Rb (339) and low Rb/Ba (0.06) ratios (Tarney and Jones, 1994). Several processes have been proposed to account for the silicic rocks with high Ba and Sr concentrations, such as mixing of mantle-derived basaltic with crust-derived felsic melts (Zhang et al., 2015) and partial melting of (1) subducted oceanic plateau (Tarney and Jones, 1994), (2) enriched lithospheric mantle metasomatized by subduction-related sedimentary fluids and/or melts (Eklund et al., 1998; Fowler et al., 2001, 2008; Yuan et al., 2010) and (3) mafic lower crust (Ye et al., 2008; Choi et al., 2009). The lack of mafic microgranular enclaves in the Triassic granodiorite implies that magma mixing between mantle- and crust-derived melts is not a plausible mechanism. Additionally, because the Ob-Zaisan Ocean was already closed in the early Triassic (Kruk et al., 2014; Chen et al., 2019a,b; Kuibida et al., 2019), formation of the high Ba–Sr granodiorite by partial melting of subducted oceanic plateaus seems unlikely. Numerous examples show that high Ba–Sr granitoids formed by differentiation are related to abundant coeval mantle-derived basaltic magmas and are characterized by high Mg#, high Sr/Y and La/Yb ratios, high Cr and Ni contents and strongly fractionated REE patterns (Eklund et al., 1998; Fowler and Rollinson, 2012; Yuan et al., 2010). However, in the late Permian to early Triassic, there was no coeval or volumetrically abundant basaltic rocks associated with this pluton. Besides, the Triassic sample of this study has relatively low Mg# (33.9), low Sr/Y (3.5) and La/Yb (5.7) ratios, low Cr (4.0 ppm) and Ni (3.9 ppm) contents and exhibits weak REE fractionation (Fig. 5e), which contrast to those originated from enriched lithospheric mantle by differentiation. When combining with previously published data for this pluton (Kruk et al., 2014), data show negative correlations of $Fe_2O_3^T$, Zr and La with SiO_2

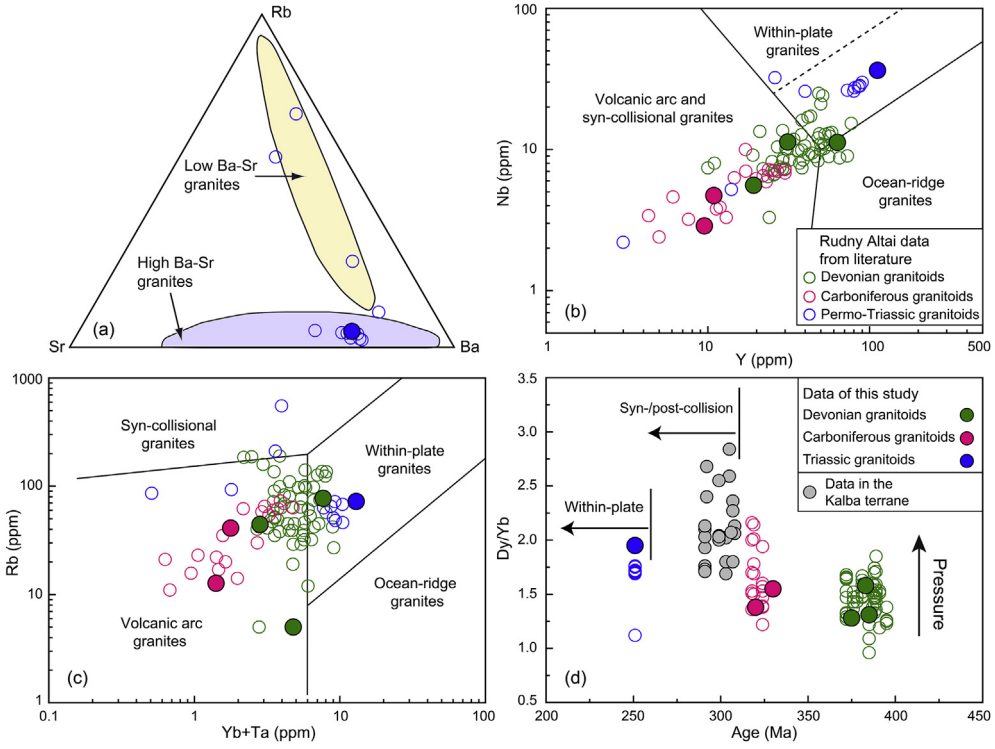

Fig. 9. (a) Sr–Rb–Ba diagram (after Tarney and Jones, 1994) for the Permo-Triassic granitoids in the Rudny Altai. (b) Nb–Y and (c) Rb–(Yb+Ta) diagrams (after Pearce et al., 1984) for the granitoids in the Rudny Altai. (d) Dy/Yb–Age diagram for the granitoids in the Rudny Altai and Kalba terrane. Rudny Altai data from literature are from Kruk et al. (2014), Kuibida et al. (2013, 2020) and Kuybida et al. (2015). The data in the Kalba terrane are from Kuibida et al. (2019).

(not shown), further arguing against the fractional crystallization process. Instead, we consider partial melting of pre-existing mafic components as a likely mechanism to generate the Triassic pluton. The derivation from melting of a basaltic component is supported by its low Rb/Ba (0.06), Rb/Sr (0.19) and Al_2O_3/TiO_2 (12.2) ratios (Fig. 8c and 8d) and metaluminous feature (A/CNK = 0.87). Actually, the intermediate SiO_2 (63.2 wt.%) and relatively high Na_2O (3.80 wt.%) and K_2O (2.94 wt.%) contents and K_2O/Na_2O (0.77) ratio of the Triassic sample are similar to experimental products of partial melting of middle to high K basaltic rocks (Sisson et al., 2005). Likewise, Roberts and Clemens (1993) experimentally demonstrated that high-K calc-alkaline granitoids can be created by partial melting of high-K calc-alkaline mafic rocks originated from enriched subcontinental lithospheric mantle. Middle to high K basaltic to dioritic rocks have been reported in the late Devonian Ust'-Belovsky complex and late Carboniferous Gilevsky and Volchikhinsky complexes (Fig. 4b), which could be the source rocks of the Triassic granodiorite.

5.3. Implications for geodynamics and evolution of continental crust

Recent studies have revealed that the Devonian to Carboniferous evolution of the Rudny Altai was linked to the northeastward subduction of the Ob-Zaisan oceanic lithosphere beneath the Siberian accretionary margin (i.e., Gorny Altai island arc and Altai–Mongolian terrane; Buslov et al., 2004; Kruk et al., 2014; Safonova, 2014). However, details of the subduction process and closure time of the Ob-Zaisan Ocean are not well constrained, despite that some scholars consider it closed in the middle Carboniferous (Kuibida et al., 2019). Comparison of granitoid ages in the Gorny Altai and Rudny Altai shows that the early Devonian granitoids (420–400 Ma) are confined to the Gorny Altai, while granitoids younger than 400 Ma occur in both units (Chen et al., 2016, 2019a; Kuibida et al., 2020). Such a migration of magmatic front may imply an episode of retreat of the subducting Ob-Zaisan oceanic plate in the Devonian (Li et al., 2019), which is supported by the development of Devonian bimodal volcanics and A-type rhyolites with high Ga/Al ratios and high Zr + Nb + Ce + Y contents (Fig. 8a and 8b; Kuibida et al., 2020) and VMS-type Cu–Zn deposits in the Rudny Altai and Altai–Mongolian terranes (Buslov et al., 2004; Dyachkov et al., 2009; Lobanov et al., 2014; Safonova, 2014; Yang et al., 2014). Therefore, it is inferred that the Devonian granitoids were probably formed in a retreating episode of subduction.

As for the middle to late Carboniferous (330–318 Ma) granitoids in the Rudny Altai, a collision-related environment has been previously invoked (Kuibida et al., 2013; Kruk et al., 2014). However, these rocks exhibit typical characteristics of arc granites such as low Nb, Y, Rb and Yb + Ta contents (Fig. 9b and 9c; Pearce et al., 1984), which imply a subduction-related rather than a collision-related setting. Indeed, multiple lines of evidence manifest that the Ob-Zaisan Ocean was not closed prior to late Carboniferous. For instance,

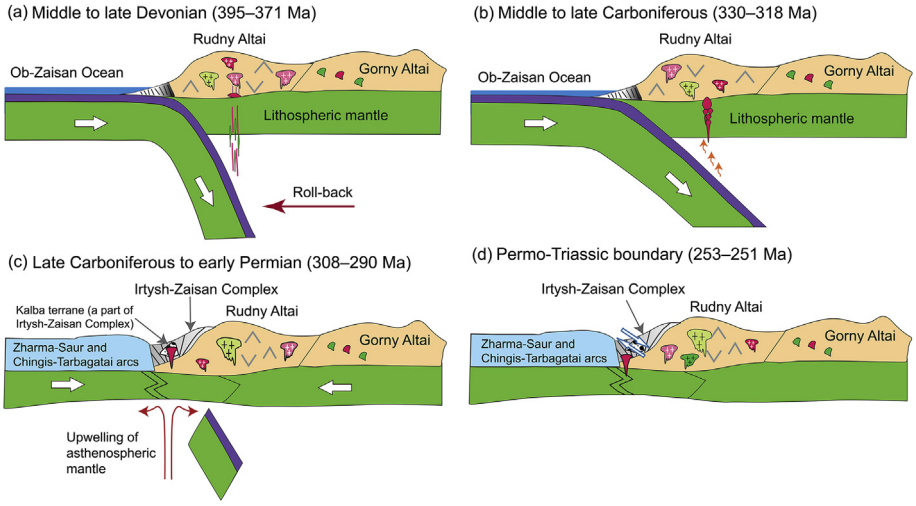

Fig. 10. Schematic cartoons illustrate the late Paleozoic to earliest Mesozoic tectonic evolutionary processes of the Rudny Altai. (a) Middle to late Devonian (395–371 Ma) northeastward subduction of the Ob-Zaisan Ocean beneath the western margin of the Siberian accretionary system (i.e., Gorny Altai) led to the formation of Rudny Altai; (b) Middle to late Carboniferous (330–318 Ma) normal subduction of the Ob-Zaisan Ocean; (c) The Altai Mountain evolved into a syn-/post-collisional stage following the closure of the Ob-Zaisan Ocean during the late Carboniferous to early Permian (308–290 Ma); (d) The Altai Mountain underwent intraplate epeirogeny at the Permo-Triassic boundary (253–251 Ma).

detrital zircon data show that the late Carboniferous clastic rocks from the Zharma–Saur arc on the southwest side of the Ob-Zaisan Ocean do not contain detrital zircons sourced from the other side (i.e., the Altai–Mongolian terrane and Gorny Altai island arc), suggesting that the Ob-Zaisan Ocean was still open during the deposition of these rocks (Li et al., 2017). The youngest age peak (ca. 323 Ma) of detrital zircons from these sequences provides a maximum time constraint for the closure of the Ob-Zaisan Ocean. Besides, the occurrence of late Carboniferous (ca. 313 Ma) subduction-related igneous rocks in the southern Altai–Mongolian terrane supports the closure of the Ob-Zaisan Ocean at some time after ~313 Ma (Cai et al., 2012). Hence, we propose that the middle to late Carboniferous (330–318 Ma) granitoids were produced in a subduction-related setting.

Since 318 Ma, late Carboniferous to early Permian magmatism vanished in the Rudny Altai, but widely intruded farther south into the Irtysh–Zaisan Complex (i.e., Kalba–Narym terrane) (Fig. 7), which represents a collisional front between the Siberian accretionary margin and Zharma–Saur/Chingis–Tarbagatai arcs (Kazakhstan collage system; Fig. 1a) (Xiao et al., 2015; Li et al., 2017; Safonova et al., 2018; Kuibida et al., 2019). Granitoids of this stage (308–290 Ma) in the Kalba terrane exhibit high Dy/Yb ratios (Fig. 9d) and probably reflect crustal thickening (Mamani et al., 2010), which can be attributed to the collisional event as the result of the closure of the Ob-Zaisan Ocean. In addition, coeval underplating of basaltic magmas was considered to create a thermal anomaly and promote partial melting of the overlying crustal rocks to form the granitoids of this stage (Khromykh et al., 2018).

In the late Permian to early Triassic (253–251 Ma), granitic magmatism in the Rudny Altai resumed, but was small in volume (Kruk et al., 2014; Gavryushkina et al., 2019). Granitoids of this period are characterized by decreasing Dy/Yb ratios (Fig. 9d) and increasing Y, Nb and Yb + Ta contents (Fig. 9b and 9c), reflecting a close tie with an intraplate setting (Pearce et al., 1984). The generation of these granitoids could be triggered by the transpressional structures which were active at ~283–253 Ma as constrained by the $^{40}Ar/^{39}Ar$ plateau ages along the Irtysh shear zone (Buslov et al., 2004; Briggs et al., 2007; Zhang et al., 2012; Li et al., 2017).

Based on the above discussion, an updated evolution model for the Rudny Altai can be illustrated. In the middle to late Devonian (395–371 Ma), a retreating episode of subduction of the Ob-Zaisan Ocean under the western margin of the Siberian accretionary system (i.e., Gorny Altai island arc and Altai–Mongolian terrane) contributed to the development of the Rudny Altai (Fig. 10a). The subduction of the Ob-Zaisan oceanic plate likely lasted until the middle to late Carboniferous (330–318 Ma) (Fig. 10b). Subsequently, following the closure of the Ob-Zaisan Ocean, the Rudny Altai evolved into a syn-/post-collisional stage accompanied by the intrusion of late Carboniferous to early Permian (308–290 Ma) granitic magmatism in the Kalba terrane (Fig. 10c). At the Permo-Triassic boundary (253–251 Ma), the Altai Mountain underwent intraplate epeirogeny that was recorded by the coevally small amounts of granitoids (Fig. 10d).

6. Conclusions

Three episodes of granitoids have been recognized in the Rudny Altai, i.e., middle to late Devonian (395–371 Ma), middle to late Carboniferous (330–318 Ma) and Permian to Triassic (253–251 Ma). Granitic magmatism of the first two episodes was generated by partial melting of a mixed source of clay-poor sediments and basaltic components in variable proportions, while that of the third episode was derived from

partial melting of middle to high K mafic crustal rocks. In addition, one episode of late Carboniferous to early Permian (308−290 Ma) granitic magmatism took place in the adjacent Kalba terrane (Kuibida et al., 2019). Combining with regional available data, we propose that the Devonian to late Carboniferous (395−318 Ma) and late Carboniferous to early Permian (308−290 Ma) magmatism respectively records the subduction and closure of the Ob-Zaisan Ocean, while the late Permian to early Triassic (253−251 Ma) granitoids are products of intraplate epeirogeny in the Altai Mountain.

Conflicts of interest

The authors of the paper declare that there is no further conflict of interest.

Acknowledgements

We thank Xianglin Tu, Shengling Sun, Xinyu Wang, Jiaqi Ling, Wanwan Hu and Xinyu Xiao for their help with the geochemical and geochronological analyses. We are very grateful to Inna Safonova for providing samples of this study. We thank Editor Weidong Sun for his kind editorial help and constructive comments. We are indebted to two anonymous reviewers, whose insightful and constructive reviews greatly improve this manuscript. This work is financially supported by the National Key R&D Program of China (2017YFC0601205), the Hong Kong RGC research projects (17303415, 17302317), the International Partnership Program of Chinese Academy of Sciences (132744KYSB20190039) and the National Science Foundation of China (41603030, 41973021, 41872222). Pengfei Li acknowledges the Thousand Youth Talents Plan and a project form Guangdong province (2019QN01H101). This is a contribution of the Chemical Geodynamic Joint Laboratory between HKU and GIG, CAS.

Appendix A. Supplementary data

Supplementary data to this article can be found online at https://doi.org/10.1016/j.sesci.2020.05.001.

References

Annen, C., Blundy, J.D., Sparks, R.S.J., 2006. The genesis of intermediate and silicic magmas in deep crustal hot zones. J. Petrol. 47, 505−539.

Barbarin, B., 1999. A review of the relationships between granitoid types, their origins and their geodynamic environments. Lithos 46, 605−626.

Bonin, B., 2007. A-type granites and related rocks: evolution of a concept, problems and prospects. Lithos 97, 1−29.

Briggs, S.M., Yin, A., Manning, C.E., Chen, Z.L., Wang, X.F., Grove, M., 2007. Late paleozoic tectonic history of the ertix Fault in the Chinese Altai and its implications for the development of the central Asian orogenic system. Geol. Soc. Am. Bull. 119, 944−960.

Brown, M., 2013. Granite: from genesis to emplacement. Geol. Soc. Am. Bull. 125, 1079−1113.

Buslov, M.M., Geng, H., Travin, A.V., Otgonbaatar, D., Kulikova, A.V., Ming, C., Stijn, G., Semakov, N.N., Rubanova, E.S., Abildaeva, M.A., Voitishek, E.E., Trofimova, D.A., 2013. Tectonics and geodynamics of Gorny Altai and adjacent structures of the Altai−Sayan folded area. Russ. Geol. Geophys. 54, 1250−1271.

Buslov, M.M., Watanabe, T., Fujiwara, Y., Iwata, K., Smirnova, L.V., Safonova, I.Y., Semakov, N.N., Kiryanova, A.P., 2004. Late Paleozoic faults of the Altai region, Central Asia: tectonic pattern and model of formation. J. Asian Earth Sci. 23, 655−671.

Cai, K.D., Sun, M., Jahn, B.M., Xiao, W.J., Yuan, C., Long, X.P., Chen, H.Y., Tumurkhuu, D., 2015. A synthesis of zircon U−Pb ages and Hf isotopic compositions of granitoids from Southwest Mongolia: implications for crustal nature and tectonic evolution of the Altai Superterrane. Lithos 232, 131−142.

Cai, K.D., Sun, M., Yuan, C., Xiao, W.J., Zhao, G.C., Long, X.P., Wu, F.Y., 2012. Carboniferous mantle-derived felsic intrusion in the Chinese Altai, NW China: implications for geodynamic change of the accretionary orogenic belt. Gondwana Res. 22, 681−698.

Chappell, B.W., White, A.J.R., 1992. I- and S-type granites in the Lachlan Fold belt. Trans. R. Soc. Edinb. Earth Sci. 83, 1−26.

Chen, M., Sun, M., Buslov, M.M., Cai, K.D., Zhao, G.C., Kulikova, A.V., Rubanova, E.S., 2016. Crustal melting and magma mixing in a continental arc setting: evidence from the Yaloman intrusive complex in the Gorny Altai terrane, central Asian orogenic belt. Lithos 252−253, 76−91.

Chen, M., Sun, M., Buslov, M.M., Zheng, J.P., Zhao, J.H., Cai, K.D., Kulikova, A.V., 2019a. Devonian continental arc intermediate-felsic magmatism in the Gorny Altai terrane, northwestern central Asian orogenic belt: heterogenous crustal melting and input of mantle melts. Lithos 332−333, 175−191.

Chen, M., Sun, M., Li, P.F., Zheng, J.P., Cai, K.D., Su, Y.P., 2019b. Late paleozoic accretionary and collisional processes along the southern peri-Siberian orogenic system: new constraints from amphibolites within the Irtysh complex of Chinese Altai. J. Geol. 127, 241−262.

Chiaradia, M., Müntener, O., Beate, B., 2014. Quaternary sanukitoid-like andesites generated by intracrustal processes (Chacana Caldera Complex, Ecuador): implications for Archean sanukitoids. J. Petrol. 55, 769−802.

Choi, S.G., Rajesh, V.J., Seo, J., Park, J.W., Oh, C.W., Pak, S.J., Kim, S.W., 2009. Petrology, geochronology and tectonic implications of Mesozoic high Ba−Sr granites in the Haemi area, Hongseong Belt, South Korea. Isl. Arc 18, 266−281.

Collins, W.J., 2002. Hot orogens, tectonic switching, and creation of continental crust. Geology 30, 535−538.

Collins, W.J., Huang, H.Q., Bowden, P., Kemp, A.I.S., 2020. Repeated S−I−A-type granite trilogy in the Lachlan Orogen and geochemical contrasts with A-type granites in Nigeria: implications for petrogenesis and tectonic discrimination. Geol. Soc. Spec. Publ. 491, 53−76.

Dyachkov, B.A., Titov, D.V., Sapargaliev, E.M., 2009. Ore belts of the greater Altai and their ore resource potential. Geol. Ore Deposits 51, 197−211.

Eklund, O., Konopelko, D., Rutanen, H., Fröjdö, S., Shebanov, A.D., 1998. 1.8 Ga Svecofennian post−collisional shoshonitic magmatism in the Fennoscandian shield. Lithos 45, 87−108.

Elburg, M., Vroon, P., van der Wagt, B., Tchalikian, A., 2005. Sr and Pb isotopic composition of five USGS glasses (BHVO-2G, BIR-1G, BCR-2G, TB-1G, NKT-1G). Chem. Geol. 223, 196−207.

Fowler, M.B., Henney, P.J., Darbyshire, D.P.F., Greenwood, P.B., 2001. Petrogenesis of high Ba−Sr granites: the Rogart pluton, Sutherland. J. Geol. Soc. London 158, 521−534.

Fowler, M.B., Kocks, H., Darbyshire, D.P.F., Greenwood, P.B., 2008. Petrogenesis of high Ba−Sr plutons from the northern highlands terrane of the British Caledonian province. Lithos 105, 129−148.

Fowler, M.B., Rollinson, H., 2012. Phanerozoic sanukitoids from Caledonian Scotland: implications for Archean subduction. Geology 40, 1079−1082.

Gao, S., Rudnick, R.L., Yuan, H.L., Liu, X.M., Liu, Y.S., Xu, W.L., Ling, W.L., Ayers, J., Wang, X.C., Wang, Q.H., 2004. Recycling lower continental crust in the North China craton. Nature 432, 892−897.

Gavryushkina, O.A., Kruk, N.N., Semenov, I.V., Vladimirov, A.G., Kuibida, Y.V., Serov, P.A., 2019. Petrogenesis of Permian-Triassic intraplate gabbro-granitic rocks in the Russian Altai. Lithos 326−327, 71−89.

Goldstein, S.L., O'Nions, R.K., Hamilton, P.J., 1984. A Sm-Nd isotopic study of atmospheric dusts and particulates from major river systems. Earth Planet Sci. Lett. 70, 221−236.

Jahn, B.M., Wu, F.Y., Chen, B., 2000. Massive granitoid generation in Central Asia: Nd isotope evidence and implication for continental growth in the Phanerozoic. Episodes 23, 82–92.

Jung, S., Pfänder, J.A., 2007. Source composition and melting temperatures of orogenic granitoids: constraints from CaO/Na_2O, Al_2O_3/TiO_2 and accessory mineral saturation thermometry. Eur. J. Mineral 19, 859–870.

Khain, E.V., Bibikova, E.V., Salnikova, E.B., Kröner, A., Gibsher, A.S., Didenko, A.N., Degtyarev, K.E., Fedotova, A.A., 2003. The Palaeo-Asian ocean in the Neoproterozoic and early Palaeozoic: new geochronologic data and palaeotectonic reconstructions. Precambrian Res. 122, 329–358.

Khromykh, S.V., Tsygankov, A.A., Burmakina, G.N., Kotler, P.D., Sokolova, E.N., 2018. Mantle-crust interaction in petrogenesis of the gabbro-granite association in the Preobrazhenka intrusion, Eastern Kazakhstan. Petrology 26, 368–388.

Kröner, A., Windley, B.F., Badarch, G., Tomurtogoo, O., Hegner, E., Jahn, B.M., Gruschka, S., Khain, E.V., Demoux, A., Wingate, M.T.D., 2007. Accretionary growth and crust formation in the central Asian orogenic belt and comparison with the Arabian–Nubian shield. Mem. Geol. Soc. Am. 200, 181–209.

Kruk, N.N., 2015. Continental crust of Gorny Altai: stages of formation and evolution; indicative role of granitoids. Russ. Geol. Geophys. 56, 1097–1113.

Kruk, N.N., Kuybida, M.L., Murzin, O.V., Gusev, N.I., Shokalsky, S.P., Vladimirov, A.G., Smirnov, S.Z., Gaskov, I.V., Travin, A.V., Khromykh, S.V., Volkova, N.I., Kuybida, Ya.V., Annikova, I.Yu., Kotler, P.D., Mikheev, E.I., 2014. Granitoids of the North-West Altai Guidebook for Field Excursion. Publishing House of Siberian Branch of the Russian Academy Sciences, p. 84p.

Kruk, N.N., Vladimirov, A.G., Babin, G.A., Shokalsky, S.P., Sennikov, N.V., Rudnev, S.N., Volkova, N.I., Kovach, V.P., Serov, P.A., 2010. Continental crust in Gorny Altai: nature and composition of protoliths. Russ. Geol. Geophys. 51, 431–446.

Kuibida, M.L., Dyachkov, B.A., Vladimirov, A.G., Kruk, N.N., Khromykh, S.V., Kotler, P.D., Rudnev, S.N., Kruk, E.A., Kuibida, Y.V., Oitseva, T., 2019. Contrasting granitic magmatism of the Kalba fold belt (East Kazakhstan): evidence for Late Paleozoic post-orogenic events. J. Asian Earth Sci. 175, 178–198.

Kuibida, M.L., Kruk, N.N., Murzin, O.V., Shokal'skii, S.P., Gusev, N.I., Kirnozova, T.I., Travin, A.V., 2013. Geologic position, age, and petrogenesis of plagiogranites in northern Rudny Altai. Russ. Geol. Geophys. 54, 1135–1148.

Kuibida, M.L., Kruk, N.N., Vladimirov, A.G., Polyanskii, N.V., Nikolaeva, I.V., 2009. U-Pb isotopic age, composition, and sources of the plagiogranites of the Kalba range, Eastern Kazakhstan. Dokl. Earth Sci. 424, 72–76.

Kuibida, M.L., Murzin, O.V., Kruk, N.N., Safonova, I.Y., Sun, M., Komiya, T., Wong, J., Aoki, S., Murzina, N.M., Nikolaeva, I., Semenova, D.V., Khlestov, M., Shelepaev, R.A., Kotler, P.D., Yakovlev, V.A., Narvzhnova, A.V., 2020. Whole-rock geochemistry and U-Pb ages of Devonian bimodal-type rhyolites from the Rudny Altai, Russia: petrogenesis and tectonic settings. Gondwana Res. 81, 312–338.

Kuybida, M.L., Kruk, N.N., Shokal'skii, S.P., Gusev, N.I., Murzin, O.V., 2015. Subduction plagiogranites of Rudny Altai: age and composition characteristics. Dokl. Earth Sci. 464, 317–322.

Le Bas, M.J., Le Maitre, R.W., Streckeisen, A., Zanettin, B., 1986. A chemical classification of volcanic rocks based on the total alkali–silica diagram. J. Petrol. 27, 745–750.

Li, P.F., Sun, M., Rosenbaum, G., Jourdan, F., Li, S.Z., Cai, K.D., 2017. Late Paleozoic closure of the Ob-Zaisan Ocean along the Irtysh shear zone (NW China): implications for arc amalgamation and oroclinal bending in the Central Asian orogenic belt. Geol. Soc. Am. Bull. 129, 547–569.

Li, P.F., Sun, M., Rosenbaum, G., Yuan, C., Safonova, I., Cai, K.D., Jiang, Y.D., Zhang, Y.Y., 2018. Geometry, kinematics and tectonic models of the Kazakhstan orocline, central Asian orogenic belt. J. Asian Earth Sci. 153, 42–56.

Li, P.F., Sun, M., Shu, C.T., Yuan, C., Jiang, Y.D., Zhang, L., Cai, K.D., 2019. Evolution of the central Asian orogenic belt along the Siberian margin from Neoproterozoic-early Paleozoic accretion to Devonian trench retreat and a comparison with Phanerozoic eastern Australia. Earth Sci. Rev. 198, 102951.

Li, X.H., Li, Z.X., Wingate, M.T.D., Chung, S.L., Liu, Y., Lin, G.C., Li, W.X., 2006. Geochemistry of the 755 Ma Mundine Well dyke swarm, northwestern Australia: part of a Neoproterozoic mantle superplume beneath Rodinia? Precambrian Res. 146, 1–15.

Lobanov, K., Yakubchuk, A., Creaser, R.A., 2014. Besshi-type VMS deposits of the Rudny Altai (central Asia). Econ. Geol. 109, 1403–1430.

Ludwig, K.R., 2003. ISOPLOT 3.00: A Geochronological Toolkit for Microsoft Excel. Berkeley Geochronology Center, California, Berkeley, p. 39.

Mamani, M., Worner, G., Sempere, T., 2010. Geochemical variations in igneous rocks of the Central Andean orocline (13°S to 18°S): tracing crustal thickening and magma generation through time and space. Geol. Soc. Am. Bull. 122, 162–182.

Maniar, P.D., Piccoli, P.M., 1989. Tectonic discrimination of granitoids. Geol. Soc. Am. Bull. 101, 635–643.

Pearce, J.A., Harris, N.B., Tindle, A.G., 1984. Trace element discrimination diagrams for the tectonic interpretation of granitic rocks. J. Petrol. 25, 956–983.

Peccerillo, A., Taylor, S.R., 1976. Geochemistry of Eocene calc–alkaline volcanic rocks from the Kastamonu area, northern Turkey. Contrib. Mineral. Petrol. 58, 63–81.

Petford, N., Cruden, A.R., McCaffrey, K.J.W., Vigneresse, J.L., 2000. Granite magma formation, transport and emplacement in the Earth's crust. Nature 408, 669–673.

Rapp, R.P., Watson, E.B., 1995. Dehydration melting of metabasalt at 8–32 kbar: implications for continental growth and crust-mantle recycling. J. Petrol. 36, 891–931.

Roberts, M.P., Clemens, J.D., 1993. Origin of high-potassium, calc-alkaline, I-type granitoids. Geology 21, 825–828.

Safonova, I., 2014. The Russian-Kazakh Altai orogen: an overview and main debatable issues. Geosci Front 5, 537–552.

Safonova, I.Y., Komiya, T., Romer, R.L., Simonov, V., Seltmann, R., Rudnev, Yamamoto, S., Sun, M., 2018. Supra-subduction igneous formations of the Char ophiolite belt, East Kazakhstan. Gondwana Res. 59, 159–179.

Sengör, A.M.C., Natal'in, B.A., Burtman, V.S., 1993. Evolution of the Altaid tectonic collage and Paleozoic crustal growth in Eurasia. Nature 364, 299–307.

Sisson, T.W., Ratajeski, K., Hankins, W.B., Glazner, A.F., 2005. Voluminous granitic magmas from common basaltic sources. Contrib. Mineral. Petrol. 148, 635–661.

Sun, M., Yuan, C., Xiao, W.J., Long, X.P., Xia, X.P., Zhao, G.C., Lin, S.F., Wu, F.Y., Kröner, A., 2008. Zircon U–Pb and Hf isotopic study of gneissic rocks from the Chinese Altai: progressive accretionary history in the early to middle Palaeozoic. Chem. Geol. 247, 352–383.

Sun, S.S., McDonough, W.F., 1989. Chemical and isotopic systematics of oceanic basalts: implications for mantle composition and processes. Geol. Soc. Spec. Publ. 42, 313–345.

Sylvester, P.J., 1998. Post-collisional strongly peraluminous granites. Lithos 45, 29–44.

Tanaka, T., Togashi, S., Kamioka, H., Amakawa, H., Kagami, H., Hamamoto, T., Yuhara, M., Orihashi, Y., Yoneda, S., Shimizu, H., Kunimaru, T., Takahashi, K., Yanagi, T., Nakano, T., Fujimaki, H., Shinjo, R., Asahara, Y., Tanimizu, M., Dragusanu, C., 2000. JNdi-1: a neodymium isotopic reference in consistency with LaJolla neodymium. Chem. Geol. 168, 279–281.

Tarney, J., Jones, C.E., 1994. Trace element geochemistry of orogenic igneous rocks and crustal growth models. J. Geol. Soc. London 151, 855–868.

Tong, Y., Wang, T., Jahn, B.M., Sun, M., Hong, D.W., Gao, J.F., 2014. Post-accretionary Permian granitoids in the Chinese Altai orogen: geochronology, petrogenesis and tectonic implications. Am. J. Sci. 314, 80–109.

Wang, T., Jahn, B.M., Kovach, V.P., Tong, Y., Hong, D.W., Han, B.F., 2009. Nd–Sr isotopic mapping of the Chinese Altai and implications for continental growth in the Central Asian Orogenic Belt. Lithos 110, 359–372.

Whalen, J.B., Currie, K.L., Chappell, B.W., 1987. A-type granites: geochemical characteristics, discrimination and petrogenesis. Contrib. Mineral. Petrol. 95, 407–419.

Wilhem, C., Windley, B.F., Stampfli, G.M., 2012. The Altaids of Central Asia: a tectonic and evolutionary innovative review. Earth Sci. Rev. 113, 303−341.

Windley, B.F., Alexeiev, D., Xiao, W.J., Kröner, A., Badarch, G., 2007. Tectonic models for accretion of the central Asian orogenic belt. J. Geol. Soc. London 164, 31−47.

Windley, B.F., Kröner, A., Guo, J., Qu, G., Li, Y., Zhang, C., 2002. Neoproterozoic to Paleozoic geology of the Altai orogen, NW China: new zircon age data and tectonic evolution. J. Geol. 110, 719−737.

Xiao, W.J., Han, C.M., Yuan, C., Sun, M., Lin, S.F., Chen, H.L., Li, Z.L., Li, J.L., Sun, S., 2008. Middle Cambrian to Permian subduction−related accretionary orogenesis of North Xinjiang, NW China: implications for the tectonic evolution of Central Asia. J. Asian Earth Sci. 32, 102−117.

Xiao, W.J., Windley, B., Sun, S., Li, J.L., Huang, B.C., Han, C.M., Yuan, C., Sun, M., Chen, H.L., 2015. A tale of amalgamation of three Permo-Triassic collage systems in Central Asia: oroclines, sutures, and terminal accretion. Annu. Rev. Earth Planet Sci. 43, 16, 1−16.31.

Ye, H.M., Li, X.H., Li, Z.X., Zhang, C.L., 2008. Age and origin of high Ba−Sr appinite−granites at the northwestern margin of the Tibet Plateau: implications for early Paleozoic tectonic evolution of the Western Kunlun orogenic belt. Gondwana Res. 13, 126−138.

Yang, F.Q., Liu, F., Li, Q., Geng, X.X., 2014. In situ LA−MC−ICP−MS U−Pb geochronology of igneous rocks in the Ashele Basin, Altay orogenic belt, northwest China: constraints on the timing of polymetallic copper mineralization. J. Asian Earth Sci. 79, 477−496.

Yuan, C., Sun, M., Xiao, W.J., Li, X.H., Chen, H.L., Lin, S.F., Xia, X.P., Long, X.P., 2007. Accretionary orogenesis of the Chinese Altai: insights from Paleozoic granitoids. Chem. Geol. 242, 22−39.

Yuan, C., Zhou, M.F., Sun, M., Zhao, Y.J., Wilde, S.A., Long, X.P., Yan, D.P., 2010. Triassic granitoids in the eastern Songpan Ganzi Fold Belt, SW China: magmatic response to geodynamics of the deep lithosphere. Earth Planet Sci. Lett. 290, 481−492.

Zhang, C.L., Santosh, M., Zou, H.B., Xu, Y.G., Zhou, G., Dong, Y.G., Ding, R.F., Wang, H.Y., 2012. Revisiting the “Irtish tectonic belt”: implications for the Paleozoic tectonic evolution of the Altai orogen. J. Asian Earth Sci. 52, 117−133.

Zhang, Y.Y., Sun, M., Yuan, C., Long, X.P., Jiang, Y.D., Li, P.F., Huang, Z.Y., Du, L., 2018. Alternating trench advance and retreat: insights from Paleozoic magmatism in the eastern Tianshan, central Asian orogenic belt. Tectonics 37, 2142−2164.

Zhang, Y.Y., Sun, M., Yuan, C., Xu, Y.G., Long, X.P., Tomurhuu, D., Wang, Y., He, B., 2015. Magma mixing origin for high Ba−Sr granitic pluton in the Bayankhongor area, central Mongolia: response to slab roll-back. J. Asian Earth Sci. 113, 353−368.

Zong, K.Q., Klemd, R., Yuan, Y., He, Z.Y., Guo, J.L., Shi, X.L., Liu, Y.S., Hu, Z.C., Zhang, Z.M., 2017. The assembly of Rodinia: the correlation of early Neoproterozoic (ca. 900 Ma) high-grade metamorphism and continental arc formation in the southern Beishan Orogen, southern Central Asian Orogenic Belt (CAOB). Precambrian Res. 290, 32−48.